

Thermal activation at moderate-to-high and high damping: finite barrier effects and force spectroscopy.

J. J. Mazo,¹ O. Y. Fajardo,¹ and D. Zueco^{1,2}

¹*Departamento de Física de la Materia Condensada and Instituto de Ciencia de Materiales de Aragón, CSIC-Universidad de Zaragoza, 50009 Zaragoza, Spain*

²*Fundación ARAID, Paseo María Agustín 36, E-50004 Zaragoza, Spain*

(Dated: 19 December 2012)

We study the thermal escape problem in the moderate-to-high and high damping regime of a system with a parabolic barrier. We present an equation which matches our numerical results accounting for finite barrier effects. We discuss some issues regarding the relation between escape rate and mean first passage time and apply our results to the study of force spectroscopy problems.

I. INTRODUCTION

Seventy years ago, Kramers¹ proposed an equation for the thermal escape of a Brownian particle out of a metastable well. This problem is considered an issue of fundamental interest and it has received great attention from an impressive number of scientific areas²⁻⁴. We present here a minor contribution to this vast field: a detailed numerical study, by using Langevin dynamics simulations, of the activation problem in the moderate-to-high and high damping regime of the system.

This work is motivated by a recent numerical study of the Kramers problem at low damping⁵. There, important finite barrier effects were described, a very slow convergence to the infinite barrier limit of the system was reported and the accuracy of the Drozdov-Hayashi theory⁶ was proved. As it is shown there, an accurate theory is of fundamental interest to understand experiments in this physical regime.

On the other side of the same coin, the high damping limit of the problem is found. This is the typical case for many of the current friction⁷⁻¹¹ and biological-physics works¹²⁻¹⁴, where escape rate is the fundamental concept to understand force spectroscopy experiments. In many of these works the Kramers result for the escape rate at high damping:

$$r_{KHD} = \frac{\omega_a \omega_b}{2\pi\gamma} e^{-\Delta U/k_B T}, \quad (1.1)$$

appears as the theoretical starting point to understand experimental results.

In his famous work¹, Kramers also derived an expression for the escape rate in the moderate to high damping limit,

$$r_{KMH D} = k_{KMH D} \times \frac{\omega_a}{2\pi} e^{-\Delta U/k_B T}, \quad (1.2)$$

where the damping dependent prefactor is given by $k_{KMH D}(\gamma/\omega_b) = [1 + (\gamma/2\omega_b)^2]^{1/2} - (\gamma/2\omega_b)$. There, ω_a and ω_b are related with the potential curvature at the well and the barrier respectively, see Fig. 1, ΔU stands for the potential barrier and γ for the damping of the system. For high damping, $\gamma/\omega_b \gg 1$, we have $k_{KHD} := \omega_b/\gamma$

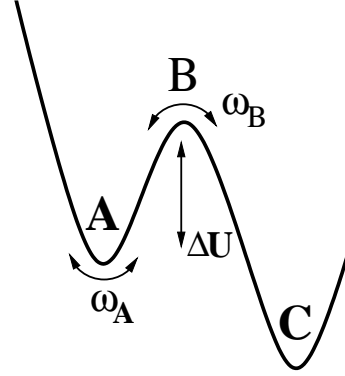


FIG. 1. Potential profile. Due to thermal fluctuations, a particle sited in state *A* is able to overcome a barrier ΔU and escape to state *C*.

for the prefactor and we recover the extensively used result of Eq. (1.1). The given results were obtained for a parabolic barrier¹⁵ in the so-called infinite barrier regime of the system, where $\Delta U/k_B T \gg 1$.

Another important concept in thermal activation theory is the mean first passage time (MFPT). This is defined as the mean time $\langle t \rangle$ for particles injected with zero velocity at point *a*, to reach a point *b*, where they are absorbed. In the overdamped limit, given the potential $U(x)$, the MFPT can be exactly computed as²

$$\langle t \rangle_{HD} = \frac{m\gamma}{k_B T} \int_a^b dy e^{U(y)/k_B T} \int_{-\infty}^y dz e^{-U(z)/k_B T}. \quad (1.3)$$

There exist an important literature studying the relation between transition rates and mean first passage times^{2,4,17,18}. It has been usually assumed, and theoretically proved, that there is a close relation between both quantities and in fact

$$r = \frac{1}{\langle t \rangle}, \quad (1.4)$$

whenever the injection and adsorbing points correspond to two potential minima separated by a barrier. Eqs. (1.3) and (1.4) allow for computing the exact escape rate in the overdamped limit of the system and for

comparing to the Kramers infinite barrier and other escape rate results.

We devote section II of the paper to this end where a critical review of existing theories is presented. There, we propose a relatively simple equation, Eq. (2.3), which allows for computing the escape rate for any barrier and damping in the moderate-to-high and high damping domains. Then, in section III we study the time to reach the barrier problem. This time, $\langle t \rangle_M$, differs from the previously calculated $\langle t \rangle$ by a factor that changes from 1 to 2 when damping increases, and it is the relevant quantity in some situations.

Armed with our previous results, we attack in section IV the so-called *force spectroscopy* problems. There, the system is continuously biased by an external field and the escape field probability distribution function is recorded. We compare results for the mean escape field based in different theories. We stress the differences between results for field to reach the next metastable state and field to reach the barrier. We also show that damping times field ramp is the relevant parameter in the overdamped limit, and that there exists a value of this parameter beyond which important nonequilibrium effects dominate the problem. We finish by showing results in the full damping spectrum.

II. MODEL AND RESULTS

We use Langevin dynamics simulations to compute the mean time for a particle with a given initial condition to reach a defined point beyond the barrier. To be precise, we will be first interested in computing the mean time for a particle sited with zero velocity in the minimum of a metastable well A to reach for first time the next available potential minimum C, see Fig. 1. For us this will be the definition of the relevant mean first passage time (MFPT) $\langle t \rangle$ of the problem.

To be definite we study the dynamics of a Brownian particle in a metastable potential:

$$m\ddot{x} + m\gamma\dot{x} = -\frac{dV}{dx} + \xi(t), \quad (2.1)$$

where for the potential we use

$$V(x) = V_0(1 - \cos x) - Fx, \quad (2.2)$$

and $\xi(t)$ is the stochastic force describing the thermal fluctuations. Here we consider white thermal noise, $\langle \xi(t) \rangle = 0$ and $\langle \xi(t)\xi(t') \rangle = 2m\gamma k_B T \delta(t - t')$.

The tilted sinusoidal potential describes a particle in a periodic potential subjected to an external field, a situation of interest in many fields. In particular, Eq. (2.1) is experimentally realized by a biased Josephson junction, and the high damping regime can be addressed with resistively shunted tunnel junctions or with superconducting-normal-superconducting ones¹⁹.

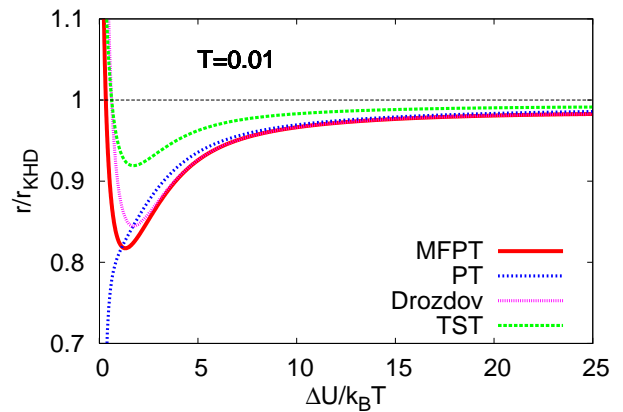


FIG. 2. (color online) Theoretical estimations of the escape rate in the high damping limit normalized by the Kramers result. Red line shows the exact mean first passage time result which accounts for the finite barrier effects in the system. We also show PT, Drozdov and exact TST results (see text and appendix).

We compute the escape rate of a particle out of the metastable well (see Fig. 1) as a function of the damping of the system and for different values of the $\delta := \Delta U/k_B T$ ratio, which is the most relevant parameter of the problem. Some authors, using different approaches, have addressed the problem of including finite barrier effects in the theory^{20–22}. This is an interesting issue since in many cases escape occurs at relatively small barriers. In our model system, the energy barrier depends on the normalized external force $f = F/V_0$ as $\Delta U = 2V_0 \left[(1 - f^2)^{1/2} - f \cos^{-1} f \right]$. Another important parameter in the theory is the value of the curvature in the metastable minimum (ω_a) and the barrier (ω_b). In this case $\omega_a = \omega_b = (V_0/m)^{1/2} (1 - f^2)^{1/4}$.

We have performed molecular dynamics simulations of Langevin equation (2.1). The equations were numerically integrated using the stochastic Runge-Kutta algorithm²³ and the MFPT was computed typically over 10000 realizations. As in our previous work⁵, we have used $m = 0.35$ and $V_0 = 0.155$. In most of the simulations we use $k_B T = 0.01$ and change F and γ .²⁴

A. High damping

First, we compare in Fig. 2 exact results from the MFPT theory [Eqs. (1.4) and (1.3)] to the Kramers infinite barrier one, Eq. (1.1). We show also the Pollak and Talkner²⁰ (PT) and Drozdov²² results, which include finite barrier corrections to the escape rates [Eq. (A5) in the appendix]. As a reference we also plot the r_{TST}^{exact} result²⁵ (see appendix). These results were proposed for the high damping limit of the system. The figure gives a quantitative estimation of the accuracy of the Kramers

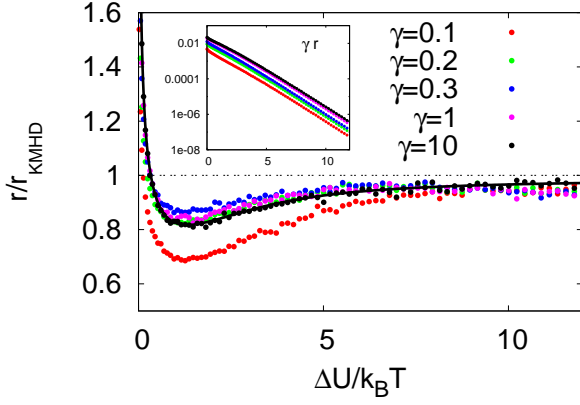


FIG. 3. (color online) Numerical estimations of the escape rate in the moderate-to-high damping regime normalized by the Kramers result of Eq. (1.2). Black line shows the exact mean first passage time result for the high damping case.

high damping result for every barrier. As it can be seen, finite barrier effects are not very severe (below 10%) for normalized barriers above 5. However some care have to be taken when considering effects involving barriers below this value. Figure also shows the convergence of the escape rate to the Kramers infinite barrier result.

As we also see in Fig. 2, PT theory gives a *simple* expression very close to the exact result except for small barriers. Drozdov gives an even better approach, however its final equation is *more complex* and only valid for very high values of the damping. PT approach fails at low barriers and Drozdov is a good approximation only in the overdamped limit.

B. Moderate-to-high damping

We propose below an expression for the escape rate which gives a good approximation for any barrier height and damping. Equation (1.3) is exact in the overdamped limit of the system. However there is no result for the MFPT at other values of the damping of the system.

Our proposal is based in observing our numerical results for the escape rate at different values of damping as a function of the normalized barrier $\Delta U/k_B T$. Figure 3 shows results for γr (inset) and r/r_{KMHD} [note that, different from Fig. 2, now we normalize the rate with respect to Eq. (1.2)] as a function of $\Delta U/k_B T$ for $T = 0.01$ and $\gamma = 0.1, 1, 10$ and 100 . There, we see first that our numerical results for high damping agree the theoretical prediction from the MFPT expression, Eq. (1.3).

Figure 3 also shows that, except for the $\gamma = 0.1$ curve (we will show below that this value of damping corresponds to the moderate damping region where $r(\gamma)$ gets a maximum), all data approximately lie in a same curve when compared to the r_{KMHD} prediction. Thus, we propose the following simple extension of the MFPT results

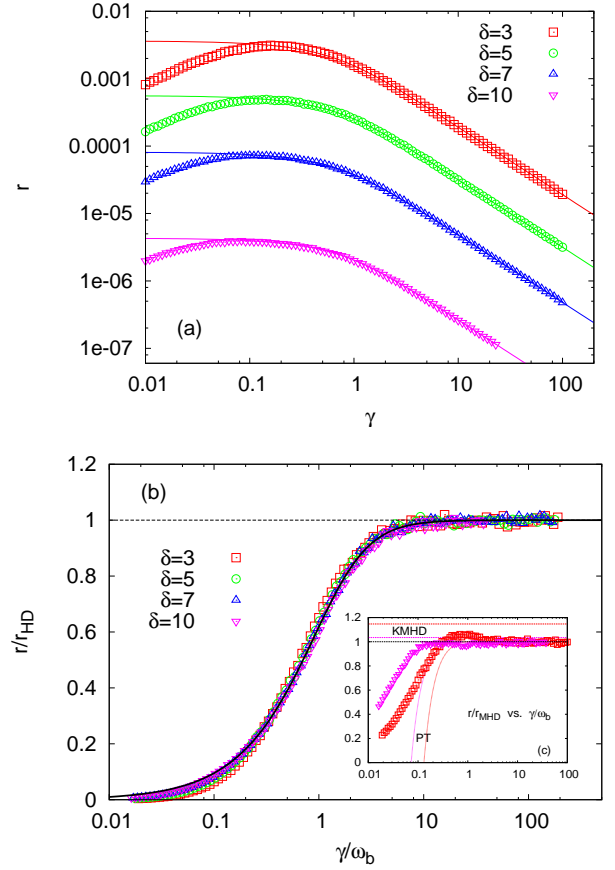


FIG. 4. (color online) Escape rate at different γ for $\delta := \Delta U/k_B T = 3, 5, 7$ and 10 , and prediction of Eq. (2.3). (a) Escape rate as a function of γ . (b) Escape rate normalized by the high damping result as a function of γ/ω_b . (c) Escape rate normalized by the result of Eq. (2.3) for $\Delta U/k_B T = 3$ and 10 and prediction of the Kramers (dashed lines) and PT (dotted lines) theories.

of Eq. (1.3) to the moderate-to-high damping region:

$$r_{MHD} = \frac{\gamma}{\omega_b} \times k_{KMHD} \left(\frac{\gamma}{\omega_b} \right) \times \frac{1}{\langle t \rangle_{HD}}. \quad (2.3)$$

The formula recovers the correct $r_{HD} = 1/\langle t \rangle_{HD}$ result for $\gamma/\omega_b \gg 1$ and incorporates the γ dependence suggested in Fig. 3. As we will see, this expression gives account of our numerical results in the moderate-to-high damping regime of the problem in a simpler and better way than any previous approach.

In order to evaluate the accuracy of Eq. (2.3), we have performed numerical simulations of the escape rate of the system as a function of γ for different values of the barrier. In particular, Fig. 4 shows our numerical results obtained for four different values of the $\Delta U/k_B T$ ratio (3, 5, 7 and 10). For better understanding, we plot results in three different ways. Figure 4(a) shows the rate versus the damping. As we see, the theoretical expression is valid for values of γ larger than 0.1 approximately.

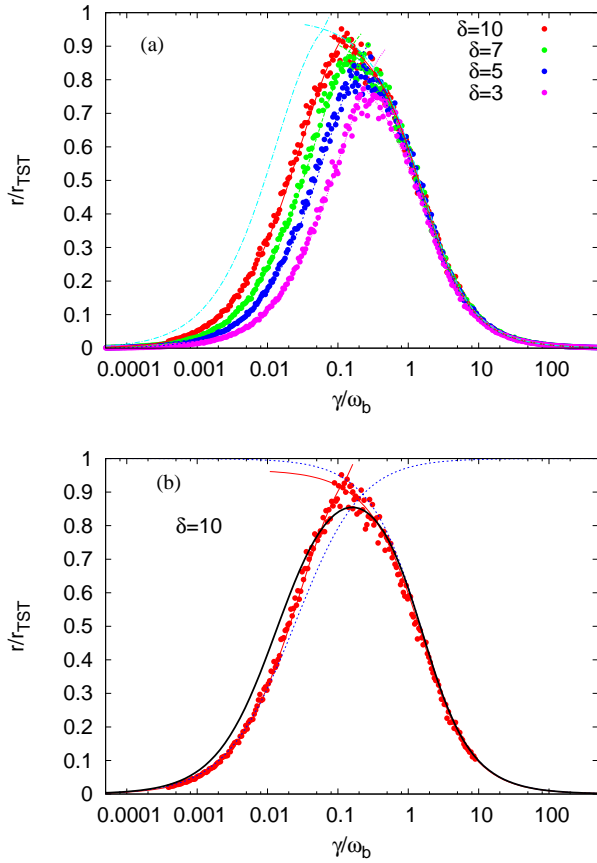


FIG. 5. (color online) (a) Theoretical (lines) and numerical (points) escape rates as a function of the normalized damping parameter for different values of the barrier over temperature ratio. Higher lines are theoretical predictions for $\Delta U/k_B T = 20$. (b) Different theoretical approaches to the escape rate and comparison to our numerical results, for $\Delta U/k_B T = 10$. Red lines stands for Drozdov-Hayashi (low damping) and for our r_{MHD} (high damping) results. Blue dotted lines stands for the BHL approach (low damping) and the KMHD one. Black line shows the simplest interpolation equation for the full damping range (see text).

This value is at the lower limit of the moderate-to-high damping region. Smaller values of γ sets in the moderate-to-low damping regime that we studied previously⁵. This kind of plots have been extensively used in the literature, however due to the log scale dependence of the rate it is unable to evaluate the precision of the theoretical equation.

Figure 4(b) plots r/r_{HD} as a function of γ/ω_b to check the validity of our ansatz in Eq. (2.3). Plotted in this way, all the curves approximately collapse in a single function given by $(\gamma/\omega_b) \times k_{KMHD}(\gamma/\omega_b)$. As expected deviations appears for the lowest values of damping.

To finish, we present in Fig. 4(c) the direct comparison of our numerical results to Eq. (2.3) and PT and Drozdov theories for $\delta = 3$ and $\delta = 10$. In this figure we plot the escape rate normalized by our theoretical expression,

r/r_{MHD} versus γ/ω_b . We conclude that Eq. (2.3) reproduces our numerical results in a better way than previous theories for any barrier and in the full moderate-to-high damping regime.

As we have seen, our numerical results are well fitted by Eq. (2.3) for damping values above $\gamma \sim 0.2$ in our units. At this intermediate values of the damping parameter we are into the so-called turnover region, which characterizes the transition between the moderate-to-low and the moderate-to-high damping regimes. There, the classical transition state theory establishes $r_{TST} = (\omega_a/2\pi) \exp -\Delta U/k_B T$.

C. Full damping

In order to supplement the information given in previous works, Fig. 5(a) shows the escape rate divided by the r_{TST} result for a wide range of damping values with special emphasis in the turnover region. As expected, when plotted as a function of the normalized damping γ/ω_b all curves collapse one each other only in the high damping limit. As barrier increases, the maximum moves to lower values of γ/ω_b . In any case rate approaches very slowly to the infinite barrier limit. The figure also shows the theoretical results studied in Ref. 5 and here. We see that the combination of the Drozdov-Hayashi⁶ result for moderate-to-low damping values and our extended mean first passage time result for the moderate-to-high ones, allows for a fairly good approximation to the numerically computed result for all damping of the system.

Fig. 5(b) shows the results for $\Delta U/k_B T = 10$ and also plots three other theoretical approaches. On the one hand we use the Kramers moderate to high damping result and the Buttiker-Harris-Landauer²⁶ (BHL) one. We see that this last deviates importantly in the moderate damping region of the system. To finish we also plot the result of the simplest analytical expression which approach the escape rate for all damping, which is given by the following interpolation formulae:

$$r_{\text{simple}}^{-1} = r_{KLD}^{-1} + r_{KMHD}^{-1}, \quad (2.4)$$

where for a linear-cubic barrier we have $r_{KLD} = (7.2\gamma/2\pi)(\Delta U/k_B T)e^{-\Delta U/k_B T}$ and r_{KMHD} is given by Eq. (1.2). This is a simple expression which, as seen in the figure, gives a first glance good idea of the escape rate behavior in the full damping spectrum of the system.

III. TIME TO REACH THE BARRIER

The general expression for the MFPT depends on the injection, a , and absorption, b , points. It is interesting to remark that the adequate choice for both numbers in order to keep Eq. (1.4) valid usually relies on relatively vague criteria since for particles starting in a metastable well *far enough* the barrier and adsorbed in another well

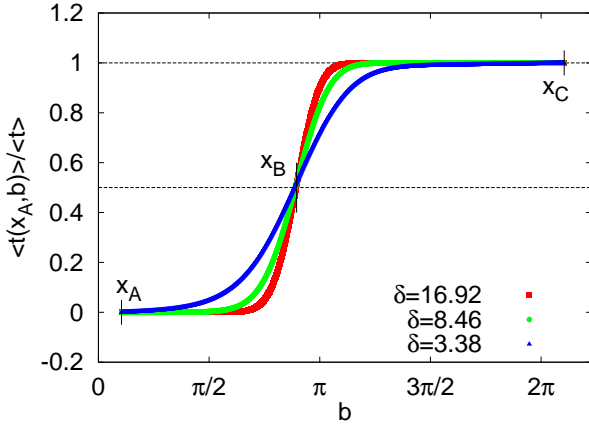


FIG. 6. (color online) Figure shows $\langle t(a, b) \rangle$ as a function of b for $a = x_A$ and $b \in (a, a + 2\pi)$. For comparison, results are normalized with respect to $\langle t \rangle = \langle t(x_A, x_C) \rangle$ for each case. We set $F = 0.05$ and plot results for three different temperatures, resulting in different $\Delta U/k_B T$ ratios. $x_A = \sin^{-1}(F/V_0)$, barrier $x_B = \pi - x_A$ and $x_C = x_A + 2\pi$ are marked by vertical segments.

well beyond the barrier, the dependence on a and b is negligible. Thus a and b should be far from the barrier. Equation (1.3) allows for a direct study of the $\langle t(a, b) \rangle$ dependence. Figure 6 explores $\langle t(a, b) \rangle$ as a function of b for $a = x_A$ (the potential minimum position) and different values of the model parameters. As it can be seen, the MFPT changes importantly in the barrier region. As expected the time to reach the next potential minimum approximately doubles the time to get the maxima. A similar study can be done to know the dependence of the MFPT on the injection position of the system, a .

There exist problems where the relevant physical magnitude is the mean time spent by the system to reach the maximum of the potential barrier (the transition state B in Fig. 1). We call here this time $\langle t \rangle^M$ to distinguish it from $\langle t \rangle$, defined above as the time to reach state C beyond the barrier.

Let us introduce the factor $\epsilon := \langle t \rangle^M / \langle t \rangle$ for the ratio between both times. As can be seen in Fig. 6, a rough estimation in the high damping limit is that $\epsilon_{HD} \simeq 0.5$, showing that a particle in the maximum has a probability close to one half to cross the barrier and close to one half to move backwards to the original well. However, this is not exactly the case and as it is well known¹⁷ the so called stochastic separatrix is sited beyond the barrier and differs from the deterministic separatrix. There, interesting dynamic effects appear in the Brownian dynamics of the system^{27,28}.

The value of $\langle t \rangle^M$ can be computed in the overdamped limit from Eq. (1.3) fixing absorption limit b at the potential barrier position. We have numerically explored how ϵ depends on the normalized barrier height $\Delta U/k_B T$ and damping of the system. We should expect a weak dependence on the barrier at high enough values of $\Delta U/k_B T$.

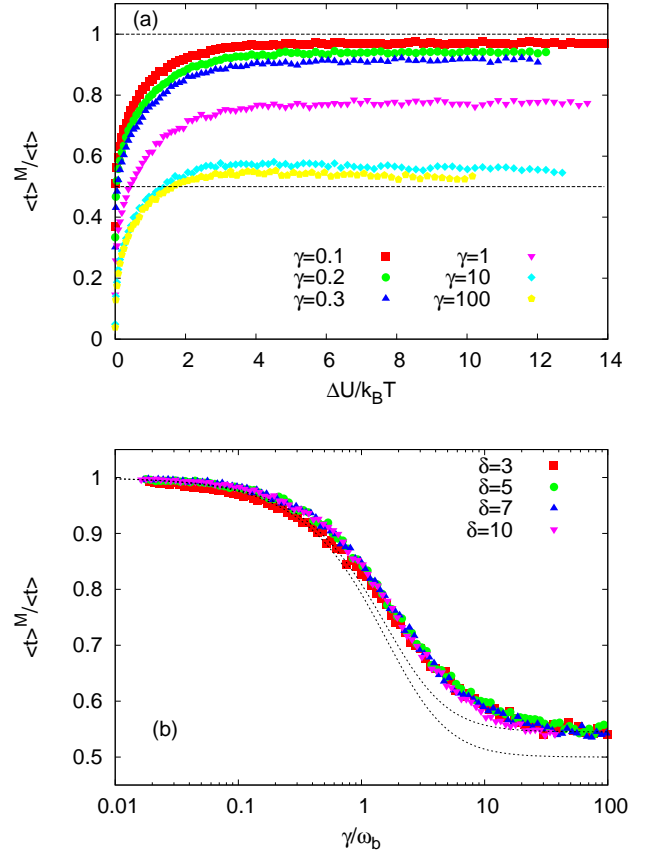


FIG. 7. (color online) $\langle t \rangle^M / \langle t \rangle$ for different values of $\Delta U/k_B T$ and γ . In (b) we also show (lines) the function proposed in Eq. (3.1) for $\epsilon_{HD} = 0.5$ and 0.545 .

With respect to the damping, ϵ changes smoothly from a value close to 0.5 for high damping to 1 for small damping. At small damping any particle that reaches the maximum has enough energy to overcome the barrier and rapidly slides down to the next potential minima.

Figure 7(a) plots ϵ as a function of $\Delta U/k_B T$ at different values of the damping γ . Figure 7(b) shows ϵ as a function of the normalized damping γ/ω_b at different values of the normalized barrier $\Delta U/k_B T$. We can see that ϵ depends very weakly on the barrier except for values of $\Delta U \leq 3k_B T$. In which respects to the damping dependence, ϵ changes from $\epsilon_{HD} \simeq 0.55$ at our parameters for $\gamma > 10$ to $\epsilon \simeq 1$ for $\gamma < 0.1$.

In a similar way that for evaluating escape rates, it would be useful to get an analytical expression to computing the mean time to reach the maximum at different values of the parameters of the system. From Fig. 7(b) we see that for every barrier we can write $\langle t \rangle^M = f(\gamma/\omega_b) \langle t \rangle$. Following the ansatz used to derive Eq. (2.3) we now propose²⁹

$$\frac{1}{\langle t \rangle_{MHD}^M} = \frac{\gamma}{\omega_b} \epsilon_{HD} \times k_{MHD} \left(\frac{\gamma}{\omega_b} \epsilon_{HD} \right) \times \frac{1}{\langle t \rangle_{HD}^M} \quad (3.1)$$

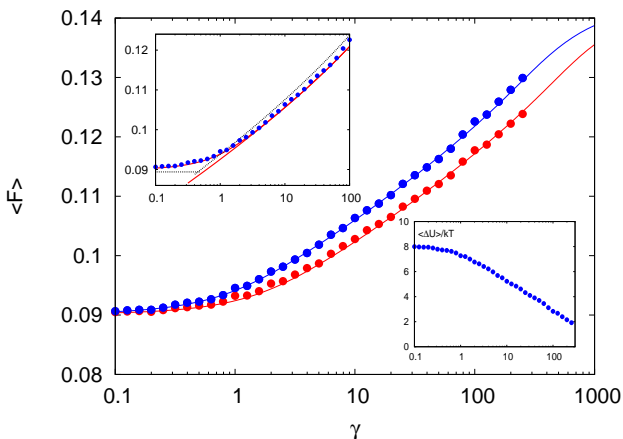


FIG. 8. (color online) Mean force $\langle F \rangle$ as a function of the damping γ for first passing the barrier top (red) and the bottom of the potential well (blue) in a force spectroscopy simulation at $T = 0.01$ and with force ramp 2.5×10^{-7} . Lines are for theoretical predictions based in Eqs. (2.3) and (3.1). Top inset: comparison to different simple theories. Bottom inset: normalized barrier at the different mean escape force values.

for the case of a parabolic barrier. There $\epsilon_{HD} = \langle t \rangle_{HD}^M / \langle t \rangle_{HD}$ is computed from Eq. (1.3). Figure 7 compares this equation to the numerical results for two possible values of ϵ_{HD} , 0.5 and 0.545. Though agreement is worse than that for the escape rate case, to our knowledge this is the first attempt to propose an expression for the $\langle t \rangle^M(\gamma)$ dependence.

IV. FORCE SPECTROSCOPY

In a typical force spectroscopy experiment the probability distribution function of the escape force $P(F)$ is measured performing many experiments where force is continuously increased at a given rate \dot{F} . From these results the mean escape force $\langle F \rangle$ and its standard deviation can be trivially computed. Such $P(F)$ can be easily related to the escape rates $r(F)$ as³⁰

$$P(F) = r(F) \left(\frac{dF}{dt} \right)^{-1} \left(1 - \int_0^F P(u) du \right). \quad (4.1)$$

Alike, escape rates can be computed from measured $P(F)$. In this section we will show results of the mean escape force in our system for different parameter conditions and compare to available theories.

As in the case of the escape rate and its relation with the MFPT, it is possible to introduce different definitions of escape force. In our simulations we start at zero force with particles in a metastable state (state A in Fig. 1) and increase the force at a given ramp. Then we define the escape force as the mean force for which particles first reach the next metastable state (state C). However, in some circumstances the relevant escape force can be

related with a different state, for instance the potential barrier (state B). In the first case we say that a particle has escaped if it has reached a new potential minimum, in the second if it has just passed the potential maximum.

Figure 8 shows the results of the mean escape force computed for both cases. As expected, $\langle F \rangle$ increases with the damping and both curves overlap for moderate damping and differ at larger ones. Figure also shows the theoretical results obtained from Eq. (4.1) with $r(F)$ computed as Eqs. (2.3) and (3.1), in this last case using $\epsilon_{HD} = 0.545$. As expected, such curves give account of the numerical results in all the studied range. We want to remark that the difference between both curves at high damping is due to the factor close to 0.5 between the MFPT for reaching states B or C. Thus, a factor of 0.5 in the prefactor of the rates have a measurable effect in the measured critical force value, see Fig. 8. This issue is not usually considered in the literature, as in many cases the prefactor is not carefully considered. In addition, some force spectroscopy experiments are interested in fact in computing forces to reach the maximum in the potential landscape of the system, the so-called transition state, B. There, results are usually analyzed at the light of the Kramers high damping result, Eq. (1.1). However, according to our previous discussion, such expression have to be corrected by a factor of 2. Such a factor is unwittingly integrated in uncertainties on the different parameters involved in the escape rate prefactor.

We also compare our results with predictions from Eqs. (1.2) and (1.1) and analytical results by Garg³¹, see appendix. Based on the small error found in the estimation of the system escape rates, we can advance that even the simplest theories give fairly good results. Such analysis is made in the top inset of Fig. 8 where the theoretical results obtained from the Kramers high damping and the Kramers moderate-to-high damping results (red lines) and the first order Garg theory (black dashed lines) for high and moderate damping are shown.

It is interesting to remark that in this numerical experiment escape happens at moderate to low values of the barrier over temperature ratio (see bottom inset in Fig. 8). Thus we see that results obtained from the infinite barrier limit give reasonable estimations for physical processes involving such small barrier values.

Next, we are going to discuss an important issue, regarding the validity of the available theories at very high damping values or force rates, where nonequilibrium effects plays a role. At high damping escape events are very rare and, if the force is varied fast enough the critical force of the model (for which barrier disappears) is reached before particles have reached the barrier. Then we can say that the escape problem is somehow ill-defined.

These observations are studied in Fig. 9 where the high $\gamma\dot{F}$ limit is reached. At high damping the probability distribution function $P(F)$ depends on \dot{F} and γ through the $\gamma\dot{F}$ product. As seen in the figure, the nonequilibrium high $\gamma\dot{F}$ regime appears in our simulations for

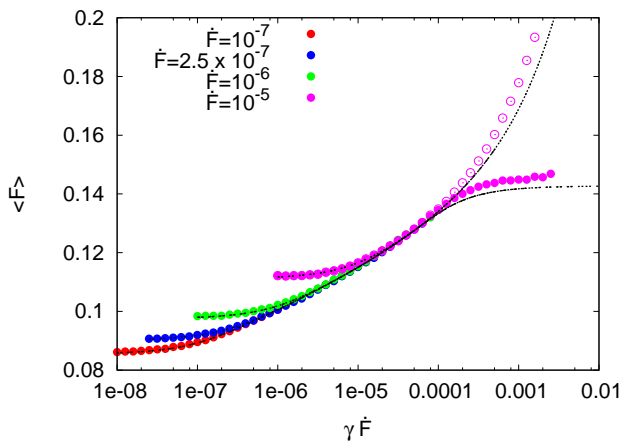


FIG. 9. (color online) Mean escape force as a function of $\gamma \dot{F}$ for different force ramps. Open and solid symbols state for two different escape force definition criteria (see text). Lines are theoretical predictions for both cases.

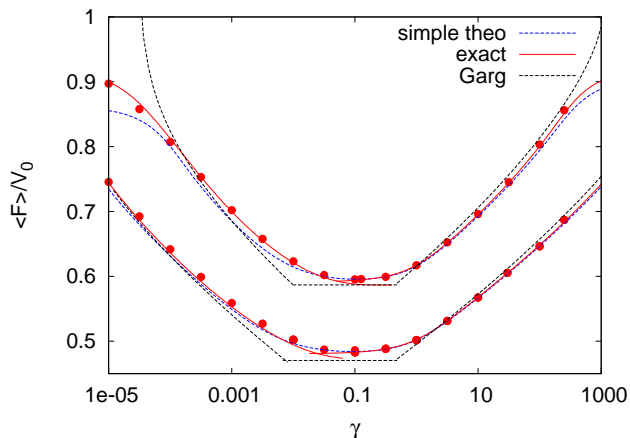


FIG. 10. (color online) Mean escape force as a function of γ for two different force ramps $\dot{F} = 10^{-8}$ (lower curve) and 3.33×10^{-7} (upper curve) and comparison with some theoretical predictions.

$\gamma \dot{F} > 10^{-4}$ ($\langle F \rangle > 0.13$ and $\Delta U/k_B T < 2$). There we observe that an increasingly important fraction of the realizations do not escape before getting the critical force value ($V_0 = 0.155$) for which the potential profile does not show a metastable well structure anymore. This situation is shown by the filled circles curves in Fig. 9 where it is plotted the mean escape force of the fraction of particles which has escaped from the potential well for $F < V_0 = 0.155$. An adequate theoretical calculation based on the MFPT results allows for reproducing the observed results even in this regime. To compare, we have also computed the mean force for the particles to advance from the starting point a to a point $b = a + 2\pi$. Result is show by open circles in the figure and, as expected, the theoretical results based in MFPT theory are also able to explain our results.

For the sake of completeness we present a plot of the normalized mean escape force for a wide range of damping values, $10^{-5} < \gamma < 10^3$ and two different force rates. As shown before, the escape rate has a maximum for $\gamma \sim 0.1$ and thus the escape force presents a minimum for such damping value. For larger values of γ our Eq. (2.3), correctly estimates the escape force. For smaller values of γ , as shown in⁵, the DH equation for low damping escape⁶ is valid. However, given the relative complexity of both approaches, we want to compare the results to those obtained with a simple interpolation formula, and the Garg analytical predictions.

The simplest analytical expression which approach the escape rate for all damping is given by the interpolation formulae of Eq. (2.4). As seen in the figure, such expression allows for a very good approach to the computation of the mean escape force. In addition, figure also shows the simple approximate published by Garg (see also appendix). We plot first order approach for moderate and high damping cases and second order for the low damping one. Such results also give a good approach to our numerical results in a wide damping area. It is important to remark now that as ramp is decreased, the moderate damping area enlarges. Thus, the border between the different damping regions is also given by the force ramp and a good knowledge of both parameters is needed to correctly understand any experimental result.

V. CONCLUSIONS AND DISCUSSION

In this article we have presented a number of results concerning the escape problem for high damping and its consequences in force spectroscopy experiments. Such problems include for instance cell to cell adhesion and molecular bond experiments^{13,33–35}, dissociation of molecular complexes³⁶, mechanical unfolding of proteins¹², single-molecule pulling experiments^{14,37–41}, free-energy reconstruction^{42–46}, and study of friction at the nanoscale^{8–11,47–49,51,52}.

Our work gives an accurate expression for escape rate in the moderate-to-high and high damping domains and allows for a quantitative evaluation of errors made in the use of different approaches to the problem. Infinite barrier results are usually assumed in literature without an estimation of the real normalized barrier values involved in any case. We have explored this issue and showed that finite barrier effects do not importantly affects force spectroscopy results though escape indeed may occur at very low barrier values (Fig. 8). This was also obtained in Ref. 50.

Another important issue is the role played by the damping parameter. This is a pretty difficult issue to evaluate in many real systems, although the validity of high damping approach is usually considered. We see that, on the one hand, high damping theories works fine for dimensionless damping $\gamma/\omega > 2$. On the other hand, if the $\gamma \dot{F}$ product goes above 10^{-4} , important non-

equilibrium effects appear and usual escape rate theories are not valid any more. We have pointed out the existence of a high $\gamma\dot{F}$ limit beyond escape problem is not well defined.

Frequently, the main source of uncertainty in the problem is the potential profile itself. Then, sometimes it is assumed $r \sim r_0 \exp(-\Delta U/k_B T)$ with r_0 some empirical prefactor. In such cases, all interest is focused on the barrier value and the field dependence of this barrier, and the *weak* r_0 dependence with F is neglected. However, in general, r_0 contains information about the damping, the bias field and the barrier shape.

In adhesion and other similar problems, free energy is frequently modeled by a tilted Morse-type potential. Then, the applied field creates a barrier³⁵. However, next potential minimum is sited at $+\infty$ and escape rate is vaguely defined in terms of being far (but not too far) from the potential barrier. Then, mean time to reach the maximum can be an useful concept and sometimes, when a cusplike barrier is assumend, it is the only meaningful one¹⁴.

We have discussed the relation between escape rate and MFPT and computed results for MFPT to the barrier. We argue that in some cases such parameter should be the relevant one. In close connection to this, in force friction experiments for instance, mean friction force is computed from the maximum force in each stick^{8,9,51,52} slip cycle. To compute such a force, the MFPT to reach the maximum is the relevant physical magnitude. This has been overlooked in the past, introducing an error by a factor of 2 in the calculus which can be easily added to the uncertainty in the evaluation of the system effective damping. This has been also the case in some analysis of single-molecule force experiments³⁸.

Most of the previously discussed issues plays also an important role when analyzing single-molecule pulling experiments^{37,40,54}. An interesting question here is that of the reconstruction of free-energy landscapes⁴². Moreover, in such, and other systems, additional issues beyond the scope of this manuscript as diffusion in a multidimensional landscape^{41,53} plays also an important role.

ACKNOWLEDGMENTS

We acknowledge F. Falo and R. Tapia-Rojo for the reading of the manuscript. This work was supported by Spain MICINN, project FIS2008-01240 and FIS2011-25167, co-financed by FEDER funds. We also thanks funding by Gobierno de Aragón.

Appendix A

Here we will give some numerical expressions that have been used along the manuscript.

1. Pollak and Talkner.

Pollak and Talkner proposed²⁰ the following expression for the escape rate:

$$r_{PT} = k_{KMH D} \times r_{TST}^{\text{exact}} \times \left(1 + \frac{f(\chi)}{x}\right) \quad (\text{A1})$$

where $x = \Delta U/k_B T$ and χ the following function of $\bar{\gamma} = \gamma/\omega_b$

$$\chi = \frac{(1 + \bar{\gamma}^2/4)^{1/2}}{\bar{\gamma}/2} \quad (\text{A2})$$

and

$$f(\chi) = \frac{1}{36\chi} \left[2 - 3\chi - \frac{1}{2}(\chi + 1)^3 + \frac{3(\chi - 1)^2(\chi + 1)(3\chi^2 + 12\chi + 1)}{9\chi^2 - 1} \right]. \quad (\text{A3})$$

In the high damping limit $\chi \rightarrow 1$ and $f(\chi) \rightarrow -5/36$ then

$$r_{PT,HD} = \frac{\omega_b}{\gamma} \times r_{TST}^{\text{exact}} \times \left(1 - \frac{5}{36x}\right). \quad (\text{A4})$$

In this theory it is necessary to compute the term

$$r_{TST}^{\text{exact}} = \left\{ \sqrt{2\pi\beta m} e^{\beta V(x_{max})} \int_{-\infty}^{x_{max}} dx e^{-\beta V(x)} \right\}^{-1}. \quad (\text{A5})$$

Note that in the high barrier limit $r_{TST}^{\text{exact}} \simeq \frac{\omega_a}{2\pi} e^{-\Delta U/k_B T} := r_{TST}$, the usual result given by the transition state theory and used in Eq. (1.2).

2. Drozdov

The problem was also studied by Drozdov in a series of papers^{6,22,32} where he proposed:

$$r_D = k_D \times r_{TST}^{\text{exact}}. \quad (\text{A6})$$

Here

$$k_D = \left[1 + \frac{\gamma^4}{\omega_e^4} \left(1 + \frac{4\theta}{n\omega_e\gamma^2} \right)^n \right]^{-1/4}, \quad (\text{A7})$$

being $n = 8/7$ a good choice,

$$\omega_e = \sqrt{2\pi/\beta} \left[\int_{-\infty}^{+\infty} dx e^{\beta V(x)} \right]^{-1}, \quad (\text{A8})$$

and

$$\theta = \frac{\omega_e^2 \beta^{3/2}}{\sqrt{2\pi}} \int_{-\infty}^{+\infty} dx V'^2(x) e^{\beta V(x)}. \quad (\text{A9})$$

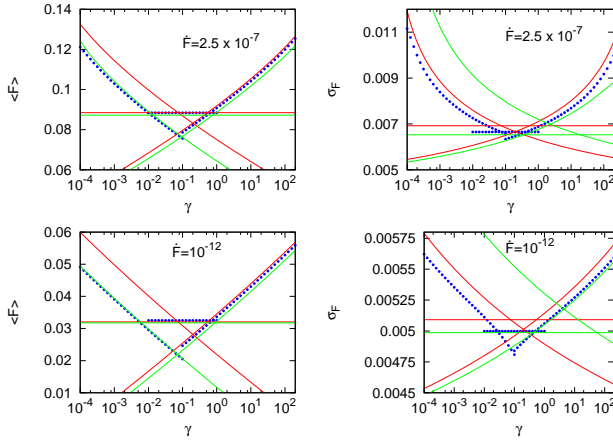


FIG. 11. (color online) Evaluation of Garg results for two different force ramps. Points stand by the exact numerical evaluation, solid lines for first order approximation, dashed lines for second order approximation results.

3. Garg

To finish, we will present a short comparative study of Garg³¹ predictions for the mean escape force and its variance. There, both quantities are given as a series expansion of a certain parameter. Figure 11 shows a numerical study of the results reported by Garg for two different force ramps. Barrier height is given by $4\sqrt{2}V_0/3(1-F/V_0)^{3/2}$, oscillation frequency by $2^{1/4}(V_0/m)^{1/2}(1-F/V_0)^{1/4}$, $T = 0.01$ and $\dot{F} = 2.5 \times 10^{-7}$ and 10^{-12} . Figure shows that for the case of $\langle F \rangle$ first order approximation is very good for the moderate and high damping cases (even better that considering the second order approximation). On the contrary, in the low damping result only the second order approximation correctly estimates the exact escape rate. With respect to the variance, result are not that good. For the case of moderate and low damping first order approximation is not that bad and second order is better. However, for low damping first order result is not good but second order is much worse.

¹H. Kramers, *Physica* **7**, 284 (1940).

²P. Hänggi, P. Talkner, and M. Borkovec, *Rev. Mod. Phys.* **62**, 251 (1990).

³V. I. Melnikov, *Phys. Rep.* **209**, 1 (1991).

⁴E. Pollak, and P. Talkner, *Chaos* **15**, 026116 (2005).

⁵J. J. Mazo, F. Naranjo, and D. Zueco, *Phys. Rev. B* **82**, 094505 (2010).

⁶A. N. Drozdov, and S. Hayashi, *Phys. Rev. E* **60**, 3804 (1999).

⁷E. Gnecco, R. Bennet, T. Gyalog, Ch. Loppacher, M. Bamberlin, E. Meyer, and H.-J. Güntherodt, *Phys. Rev. Lett.* **84**, 1172 (2000).

⁸Y. Sang, M. Dubé, and M. Grant, *Phys. Rev. Lett.* **87**, 174301 (2001).

⁹M. Evstigneev, and P. Reimann, *Europhys. Lett.* **67**, 907 (2004).

¹⁰M. Evstigneev, A. Schirmeisen, L. Jansen, H. Fuchs, and P. Reimann, *Phys. Rev. Lett.* **97**, 240601 (2006).

¹¹I. Barel, M. Urbakh, L. Jansen, and A. Schirmeisen, *Phys. Rev. Lett.* **104**, 066104 (2010).

¹²C. Hyeon, and D. Thirumalai, *Proc. Natl. Acad. Sci. U.S.A.* **100**, 10249 (2003).

¹³O. K. Dudko, A. E. Filippov, J. Klafter, and M. Urbakh, *Proc. Natl. Acad. Sci. U.S.A.* **100**, 11378 (2003).

¹⁴G. Hummer and A. Szabo, *Biophys. J.* **85**, 5 (2003).

¹⁵It worths to mention that there exist interesting problems where the parabolic barrier approach is not valid and other approaches have to be considered^{1,14,16}.

¹⁶J. L. Alonso et al., A. Castro, J. Clemente-Gallardo, P. Echenique, J. J. Mazo, V. Polo, A. Rubio, and D. Zueco, *J. Chem. Phys.* **137**, 22A533 (2012).

¹⁷R. Müller, P. Talkner, and P. Reimann, *Phys. A* **247**, 338 (1997).

¹⁸P. Reimann, G. J. Schmid, and P. Hänggi, *Phys. Rev. E* **60** R1 (1999).

¹⁹A. Barone and G. Paternó, *Physics and applications of the Josephson effect*, Wiley (1982).

²⁰E. Pollak and P. Talkner, *Phys. Rev. E* **47**, 922 (1993).

²¹V. I. Melnikov, *Phys. Rev. E* **48**, 3271 (1993).

²²A. N. Drozdov, *J. Chem. Phys.* **111**, 6481 (1999).

²³E. Helfand, *Bell Syst. Tech. J.* **58**, 2289 (1979) and H. S. Greenside and E. Helfand, *Bell Syst. Tech. J.* **60**, 1927 (1981).

²⁴To normalize Eq. (2.1) we divide it by V_0 and time by $\omega^{-1} = \sqrt{m/V_0}$. Then, the dimensionless parameters are $\tilde{\gamma} = \gamma/\omega = 1.50\gamma$, $\tilde{T} = k_B T/V_0 = 6.45k_B T$ and $\tilde{F} = \dot{F}/(\omega V_0) = 9.70\dot{F}$.

²⁵ r_{KHD} , Eq. (1.1), results from the infinite barrier approximation to r_{TST}^{exact} for parabolic barrier.

²⁶M. Büttiker, E. P. Harris, and R. Landauer, *Phys. Rev. B* **28**, 1268 (1983).

²⁷A. Fiasconaro, B. Spagnolo, and S. Boccaletti, *Phys. Rev. E* **72**, 061110 (2005).

²⁸A. Fiasconaro, J. J. Mazo, and B. Spagnolo, *Phys. Rev. E* **82**, 041120 (2010).

²⁹This is equivalent to say $\langle t \rangle^M / \langle t \rangle = k_{KMHD}(\gamma/\omega_b)/k_{KMHD}(\epsilon_{HD}\gamma/\omega_b)$.

³⁰T. A. Fulton, and L. N. Dunkleberger, *Phys. Rev. B* **9**, 4760 (1974).

³¹A. Garg, *Phys. Rev. B* **51**, 15592 (1995).

³²A. N. Drozdov, *Phys. Rev. E* **62** 1879 (2000).

³³G. I. Bell, *Science* **200**, 618 (1978).

³⁴J. Husson, and F. Pincet, *Phys. Rev. E* **77**, 026108 (2008).

³⁵L. B. Freund, *Proc. Natl. Acad. Sci. U.S.A.* **106**, 8818 (2009).

³⁶H. J. Lin, H. Y. Chen, Y. J. Sheng, and H. K. Tsao, *Phys. Rev. Lett.* **98** 088304 (2007).

³⁷O. K. Dudko, G. Hummer, and A. Szabo, *Phys. Rev. Lett.* **96**, 108101 (2006).

³⁸A. Maitra and G. Arya, *Phys. Rev. Lett.* **104** 108301 (2010).

³⁹A. Maitra and G. Arya, *Phys. Chem. Chem. Phys.* **13**, 1836 (2011).

⁴⁰S. Luccioli, A. Imparato, S. Mitternacht, A. Irbæk, and A. Torcini, *Phys. Rev. E* **81**, 010902 (2010).

⁴¹Y. Suzuki and O. K. Dudko, *Phys. Rev. Lett.* **104**, 048101 (2010).

⁴²G. Hummer and A. Szabo, *Proc. Natl. Acad. Sci. U.S.A.* **98**, 3658 (2001).

⁴³D. J. Walles and T. Head-Gordon, *J. Phys. Chem. B* **116** 8894 (2012).

⁴⁴N. C. Harris, Y. Sang, and C. H. Kiang, *Phys. Rev. Lett.* **99** 068101 (2007).

⁴⁵G. Hummer and A. Szabo, *Proc. Natl. Acad. Sci. U.S.A.* **107**, 21441 (2010).

⁴⁶R. Tapia-Rojas, D. Prada-Gracia, J. J. Mazo, and F. Falo, *Phys. Rev. E* **86**, 021908 (2012).

⁴⁷S. Y. Krylov, and J. W. M. Frenken, *J. Phys. Condens. Matter* **20**, 354003 (2008).

⁴⁸O. Y. Fajardo, and J. J. Mazo *Phys. Rev. B* **82**, 035435 (2010).

⁴⁹A. Vanossi, N. Manini, M. Urbakh, S. Zapperi, and E. Tosatti, *Rev. Mod. Phys.*, to appear.

⁵⁰J. Husson, M. Dogterom, and F. Pincet, *J. Chem. Phys.* **130**, 051103 (2009).

⁵¹A. Schirmeisen, L. Jansen, and H. Fuchs, *Phys. Rev. B*, **71**, 245403 (2005).

⁵²Y. Sang, M. Dub, and M. Grant, Phys. Rev. E **77**, 036123 (2008).

⁵³R. B. Best, and G. Hummer, Proc. Natl. Acad. Sciences **107**,

1088 (2010)

⁵⁴Z. Tshiprut, and M. Urbakh, J. Chem. Phys. **130**, 084703 (2009).